






ORIGINAL ARTICLE

The production of *terra sigillata* in Arezzo, Central Italy: an archaeometric investigation

Maria Emanuela Mascaro¹  | Emma Cantisani²  |
Marilena Ricci³  | Pasquino Pallecchi⁴ | Silvia Vilucchi⁴ |
Maria Chiara Dalconi¹  | Lara Maritan¹ 

¹Department of Geosciences, University of Padova, Padova, Italy

²CNR-ISPSC—Institute of Heritage Science (Florence Unit), Sesto Fiorentino, Italy

³Department of Chemistry “Ugo Schiff”, University of Florence, Sesto Fiorentino, Italy

⁴Superintendence Archaeology, Fine Arts and Landscape for the Metropolitan City of Florence and the Provinces of Pistoia and Prato, Florence, Italy

Correspondence

Maria Emanuela Mascaro, Department of Geosciences, University of Padova, Via G. Gradenigo 6, 35131 Padova, Italy.
Email: mariaemaneuela.mascaro@phd.unipd.it

Funding information

University of Padova

Abstract

This work deals with the archaeometric investigation on 25 fragments of *terra sigillata* (red-coated ceramic ware and moulds) found in the city of Arezzo, Tuscany (central Italy), and attributed to several important workshops from the first century BCE to the second century CE. Optical and spectroscopic techniques were used to analyse both the ceramic bodies and the red slips. All the potsherds showed a very fine-grained ceramic body, sharing similar mineralogical compositions, mainly consisting in quartz, plagioclase, pyroxene, hematite, K-feldspars, and illite/muscovite. The mineralogical data suggest that both the red-coated wares and the moulds were produced using the same calcareous-illitic clay and fired under oxidising conditions at temperatures between 850°C and 1000°C. A K-rich illitic clay with a Fe content around 10–15% (in wt%) was used to elaborate the slips. Al-substituted hematite was found in red slips by micro-Raman spectroscopy. Comparison of the chemical data with *terra sigillata* from other important production areas in Italy and from other regions of the Mediterranean Sea, allowed to define that the studied samples, locally produced in Arezzo, differ systematically from all others, although they show similarities with nearby Pisan productions as well as those Puteolan.

KEYWORDS

micro-Raman spectroscopy, production technology, red slips, *terra sigillata*, X-ray diffraction, X-ray fluorescence

This is an open access article under the terms of the [Creative Commons Attribution-NonCommercial-NoDerivs](https://creativecommons.org/licenses/by-nc-nd/4.0/) License, which permits use and distribution in any medium, provided the original work is properly cited, the use is non-commercial and no modifications or adaptations are made.

© 2024 The Author(s). *Archaeometry* published by John Wiley & Sons Ltd on behalf of University of Oxford.

INTRODUCTION

Archaeological excavations carried out in the second half of the 19th century in the complex of Santa Maria in Gradi and the surrounding areas of the city of Arezzo, Tuscany, central Italy (Figure 1a), brought to light the structural remains of ceramic workshops and drains along with a huge amount of *terra sigillata* (red-slip ware type). This particular thin tableware pot, characterised by a glossy red coating and decorations, and stamps in relief on the surface, is one of the best examples of how standardised shapes and appearance allow the identification of fairly defined chronological periods, favouring a deeper understanding and interpretation of archaeological remains (Leon et al., 2015). *Terra sigillata* ware was extensively produced in

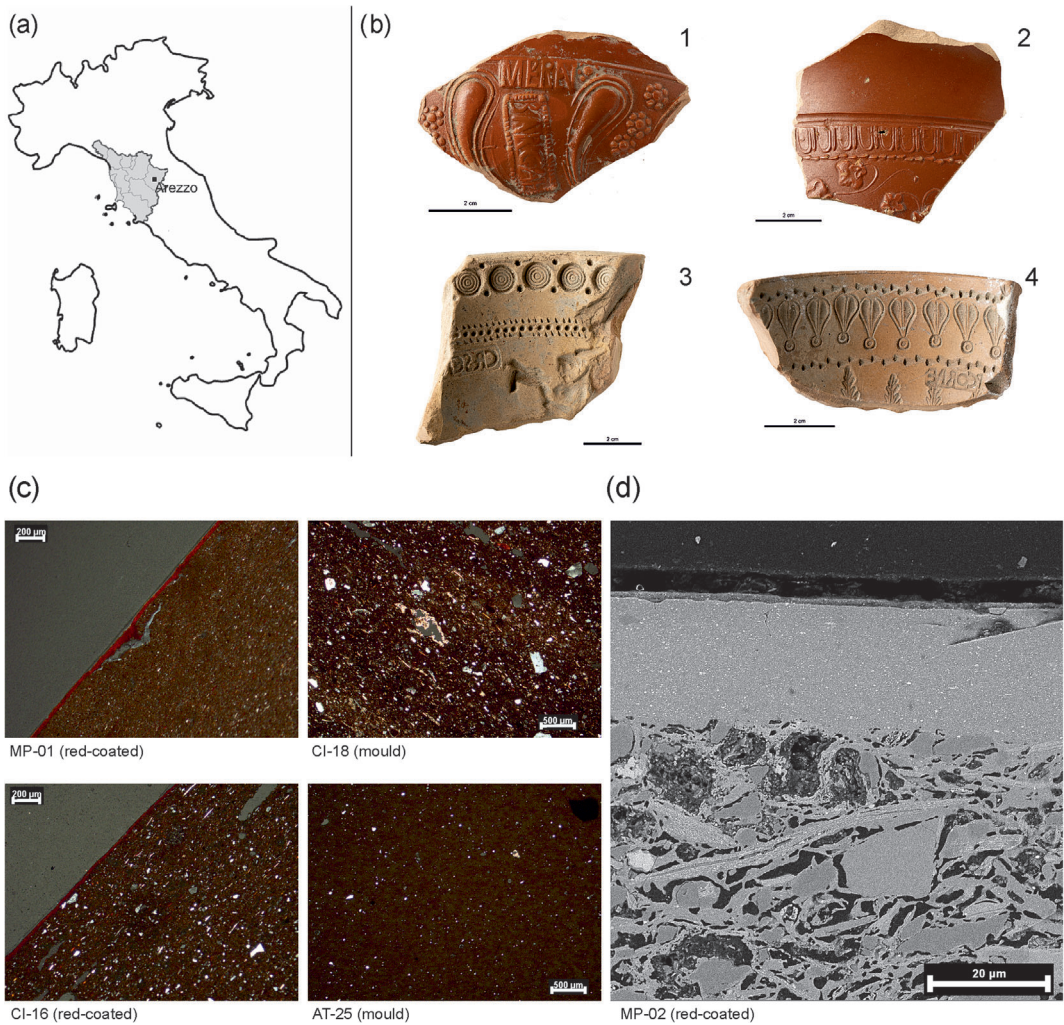


FIGURE 1 (a) Geographic location of Arezzo, Tuscany region (in grey), Central Italy. (b) Four representative samples of terra sigillata wares found in Arezzo, analysed here: (1) PB-06 signed *MERA BARGATHES*; (2) AT-23, attributed to Ateius; (3) PC-13 signed *CRESENI*; (4) CO-21 signed *PCORNE*. (c) Microphotographs of four representative samples, (two red coated and two moulds) in crossed-polarised light in which a different grain size is evident in samples CI-16 and CI-18. (d) SEM-BSE image of the sample MP-02, in which it is remarkable the compactness and good adherence of the slip (about 20 µm thick) to the ceramic body.

various regions of the Roman Empire, and from the mid-first century BCE until the beginning of the second century CE, the *italic terra sigillata* (referring with this term to the *terra sigillata* produced in Italy) was involved in all the commercial dynamics of the Roman economy. It is important to emphasise that in Arezzo, during the second century BCE, a type of black-glazed pottery was also produced. The black-glazed production had already spread during the third century BCE in central Tyrrhenian Italian peninsula founding its greatest expressions in the large productions in the area of Cales (nowadays Caserta) (Verde et al., 2022). Therefore, the red-glazed ceramic production in Arezzo is the result of a transition from black to red, through continuous technological advances by the *aretine* potters. This transformation in ceramic production perfectly fits into the context of the historical transition that, in the first century BCE, witnessed the Roman world moving to the “Augustan Age” (Morel, 2009), during which the city of Arezzo reached its peak as one of the greater production centres of *terra sigillata* wares. In this period *terra sigillata*, quickly achieved enormous commercial success and widely spread throughout all the provinces of the Roman Empire and the Mediterranean basin (Brando, 2008; Guerrini & Mancini, 2007). This allowed the birth and development of new branch workshops in various strategic centres such as Pisa (Tuscany, central Italy) and La Graufesenque (south-western France) (Lofrumento & Zoppi, 2004; Picon et al., 1975). The term *sigillata* stems from the presence of stamps or “seals” (*sigilla*) bearing the signature of the workshop’s owner and their subordinated artisans. Production techniques were so advanced as to allow mass production in sufficient quantities to meet the demands of the export market (Sciau et al., 2020). In the production of relief-decorated pots, a preparatory vase matrix was made on the lathe and used as a mould to obtain the desired shape for the final product. The decorative elements were impressed in negative on the inner surface of the vase matrix through the use of convex punches. After drying and firing, the vase matrix was used for the standardized series production of ceramic tableware for food and beverage consumption. The decorative motifs in relief on the outer surfaces of these vessels were obtained by adhering the plastic clay (leather hard) to the inner walls of the moulds by filling the cavities left by the punches, bearing the sequence of the decorations. The leather-hard vessels were coated by dipping or brushing and, after drying, fired in an oxidising atmosphere (Mirti et al., 1999; Sciau et al., 2020). The selection and appropriate treatment of clays played a key role in the development of slip quality. Whether the suspension used for the coating corresponded to the finest fraction of the clays used for ceramic bodies or to a different raw material is still a matter of debate (see Sciau et al., 2020, and references therein). The artefacts found in Arezzo belong to several important ceramic workshops characterised by a perfectly acquired production process of a pre-industrial organisation. The most famous was that of *Marcus Perennius*, located in the complex of Santa Maria in Gradi, in the centre of Arezzo. Since 15 BCE, *Perennius Tigranus* was the new owner of the same workshop, followed by *Bargathes*, 10–5 BCE, whereas the latest productions are signed by *Perennius Crescens* and *Perennius Saturnius*, the last workshop owners since 30–40 CE until the decline of the decorated production in Arezzo (Sternini, 2012). In the present study, fragments from each of the above-mentioned periods were analysed, including some potsherds from Cincelli, where a branch of the headquarters of *S. Maria* in Gradi was located, and some signed by other important Arezzo’s producers such as *Cornelius* and *Ateius*. A series of representative samples, consisting of inner decorated moulds and red-coated wares, dating from around 30 BCE to 30 CE, were analysed using a multi-analytical approach, combining microscopic, chemical, and mineralogical analyses. For the first time, it was possible to compare the ceramic fabrics of the red-coated samples with those of the moulds in terms of production technology, from the clay selection and processing, to the firing. Differences and similarities between the various workshops in Arezzo were also investigated. The examination of the red coatings was conducted to study their main features (such as thickness, colour, and appearance) and composition, focusing on the presence and type of the hematite phase. All results were also

considered from a broader perspective, comparing them with the most important *terra sigillata* wares from regional and non-regional production centres.

MATERIALS AND METHODS

Twenty-five sherds of *terra sigillata aretina* (hereafter TSA), made available by the National Archaeological Museum of Arezzo, were selected for mineralogical and chemical characterization (Figure 1b). All the fragments, consisting of 15 internally decorated moulds and 10 red-coated wares with the typical red-glossy coating on both surfaces and external relief decorations, were denominated according to the belonging workshop (Table 1), considering that the same stamps and decorations generally correspond to the same production centre (Menchelli, 2005). The area of findings and the decorative patterns on the ceramic surfaces were also considered for the discrimination of similar sherds. After being carefully cut, the freshly broken surfaces were observed with a Zeiss Stemi 2000-C stereomicroscope to compare the ceramic bodies of the samples from the different workshops. Thin section observation was performed using a Zeiss Axioscope A1 equipped with a high-resolution camera and Axiovision

TABLE 1 List of the studied samples with the type of ceramic (red-coated or mould), the stamp (if any), the site of finding and the chronological framework (Menchelli, 2005; Sternini, 2012).

Sample	Type	Workshop	Stamp	Site of finding	Chronology
MP-01	Red-coated	Marcus Perennius	-	<i>S. Maria</i> in Gradi (Arezzo)	~30–15 BCE
MP-02	Red-coated	Marcus Perennius	-	<i>S. Maria</i> in Gradi (Arezzo)	~30–15 BCE
MP-03	Mould	Marcus Perennius	-	<i>S. Maria</i> in Gradi (Arezzo)	~30–15 BCE
MP-04	Mould	Marcus Perennius	<i>Cerdo</i>	<i>S. Maria</i> in Gradi (Arezzo)	~30–15 BCE
PB-05	Mould	Perennius Bargathes	-	<i>S. Maria</i> in Gradi (Arezzo)	~10–5 BCE
PB-06	Red-coated	Perennius Bargathes	<i>MeralBargathes</i>	<i>S. Maria</i> in Gradi (Arezzo)	~10–5 BCE
PB-07	Mould	Perennius Bargathes	<i>Bargathes</i>	<i>S. Maria</i> in Gradi (Arezzo)	~10–5 BCE
PT-08	Mould	Perennius Tigranus	-	<i>S. Maria</i> in Gradi (Arezzo)	~15–10 BCE
PT-09	Mould	Perennius Tigranus	-	<i>S. Maria</i> in Gradi (Arezzo)	~15–10 BCE
PT-10	Red-coated	Perennius Tigranus	<i>Tigrani</i>	<i>S. Maria</i> in Gradi (Arezzo)	~15–10 BCE
PC-11	Red-coated	Perennius Crescens	<i>Creseni</i>	<i>S. Maria</i> in Gradi (Arezzo)	~25–30 CE
PC-12	Mould	Perennius Crescens	-	<i>S. Maria</i> in Gradi (Arezzo)	~25–30 CE
PC-13	Mould	Perennius Crescens	<i>Creseni</i>	<i>S. Maria</i> in Gradi (Arezzo)	~25–30 CE
PS-14	Red-coated	Perennius Saturnius	-	<i>S. Maria</i> in Gradi (Arezzo)	~25–30 CE
PS-15	Mould	Perennius Saturnius	<i>Saturn</i>	<i>S. Maria</i> in Gradi (Arezzo)	~25–30 CE
CI-16	Red-coated	Cincelli	<i>Tig</i>	Cincelli	~15–10 BCE
CI-17	Mould	Cincelli	-	Cincelli	Prior to 10 BCE
CI-18	Mould	Cincelli	-	Cincelli	Prior to 10 BCE
CO-19	Red-coated	Cornelius	-	Cincelli	Prior to 10 BCE
CO-20	Red-coated	Cornelius	-	Cincelli	Prior to 10 BCE
CO-21	Mould	Cornelius	<i>P Corne</i>	Cincelli	Prior to 10 BCE
CO-22	Mould	Cornelius	<i>P Coreli</i>	Cincelli	Prior to 10 BCE
AT-23	Red-coated	Ateius	-	Via Nardi (Arezzo)	~15 BCE-30 CE
AT-24	Mould	Ateius	-	Via Nardi (Arezzo)	~15 BCE-30 CE
AT-25	Mould	Ateius	-	Via Nardi (Arezzo)	~15 BC-30 CE

software for image acquisition and management. The petrographic analysis of the ceramic body was carried out following the characterisation and description methods of Quinn (2022) and Maritan (2024). Mineralogical analysis was performed on both the bodies and the coatings, mechanically separated from each other, avoiding possible contamination, and ground in an agate mortar. X-ray powder diffraction (XRPD) was carried out using a Malvern PANalytical X'Pert PRO diffractometer in Bragg–Brentano geometry, equipped with a Cu X-ray tube operating at 40 kV and 40 mA (CuK α radiation), and an X'Celerator detector. Data acquisition was performed by operating a continuous scan from 3° [2 θ] to 70° [2 θ] at an acquisition rate of 0.02° [2 θ] per second. Silicon zero-background holders were used for slip powders, due to the small quantity of material available, and a CoK α radiation was employed. HighScore Plus® 3.0 software by Malvern PANalytical was used to interpret the diffraction patterns and qualitatively analyse the mineral associations by comparison with reference patterns of the PDF database from the International Centre for Diffraction Data (ICDD). Statistical treatment of the XRPD data was performed by cluster analysis on the Quadratic Euclidean Distance according to Maritan et al. (2015), in order to group samples on the basis of their mineralogical patterns. The dissimilarity cut-off used to define the number of clusters was calculated with the KGS test (Kelley et al., 1996; Piovesan et al., 2013). A semiquantitative estimation of the crystalline phases of the pastes was performed on the XRPD data of the most representative samples of each group, using the Rietveld method as implemented in Profex 5.2.1 program (Döbelin & Kleeberg, 2015). In the Rietveld analysis of the XRPD data, the calculated crystalline phases can be taken as an overall amount, omitting the amorphous part but risking altering the percentage ratio between the various crystalline phases. The quantification of the amorphous content via X-ray diffraction can be determined using direct or indirect methods. With the indirect methods, the absolute abundances of the crystalline components are derived using a normalisation constant (e.g. internal standard or external standard method), and the amorphous content is estimated by difference. With the direct methods, the contribution of the amorphous component to the pattern is directly modelled and used to obtain an estimation of its concentration. Within indirect methods, the internal standard, consisting in the addition of a known amount of crystalline standard to the sample (De La Torre et al., 2001), is the most frequently used for the quantification of the amorphous phase. Unfortunately, the powders of the studied potsherds were no longer available, and there was not the authorization to take any more samples from the original fragments. Therefore, given the impossibility of performing the analysis with internal standard on all samples, the Rietveld analysis was carried out using the reference structure “silicabgm”, present in the Profex software's BGMN database, which takes into account the amorphous fraction by fitting the wide hump in the background of each diffractogram. The “silicabgm” approach belongs to the direct methods group and is based on the modelling of the amorphous phase starting from a crystal structure and allowing the crystallite size and strain to refine to values suitable for the broad peak widths and shapes of the observed data (Madsen et al., 2011). Although not a particularly accurate absolute quantification method, it is nevertheless effective for semiquantitative estimation of crystalline phases, bringing percentages to more reliable values and providing information on the amorphous part, which would otherwise be excluded from the analysis. All the samples were also chemically analysed in terms of their major, minor (SiO₂, TiO₂, Al₂O₃, Fe₂O₃, MnO, MgO, CaO, Na₂O, K₂O, P₂O₅), and trace elements (Sc, V, Cr, Co, Ni, Cu, Zn, Ga, Rb, Sr, Y, Zr, Nb, Ba, La, Ce, Nd, Pb, Th, U) by X-ray fluorescence (XRF), using a sequential WDS Panalytical Zetium spectrometer, equipped with a Rh tube and operating at 2.4 kW as maximum power. Samples were prepared as beads by mixing calcined powder and Li₂B₄O₇ in a 1:10 dilution ratio. The chemical elements were processed with multivariate statistical methods by principal component analysis (PCA) on the covariance matrix using STATGRAPHICS Centurion Version 19.4.02 software package in order to define differences or analogies between moulds and red-coated ceramic bodies composition and for comparison with literature data from other *terra sigillata*

production centres. The R Project for Statistical Computing was used to explore the compositional variation matrix, according to the method of Buxeda i Garrigos (1999) to determine the compositional variability for chemical elements also evaluating any possible contamination. PCA was performed on a subset of elements, excluding those with a high ratio between total variation (vt) and variance ($\tau.i.$). Raw data were standardised according to the procedures of Vitali and Franklin (1986) and Baxter (1999, 2006) by log transformation in order to avoid misclassifications due to the differing orders of magnitude and ranges of variables and also to avoid the constant sum problem (Aquilina et al., 2015). For a more in-depth observation of the coatings, a microstructural analysis was performed on polished carbon-coated sections of some representative samples using the FEG-FIB SEM TESCAN SOLARIS. Imaging was performed with the Mid-Angle-BSE in-beam detector, an acceleration voltage of 5 KeV and a current of 300 pA, with a working distance of 4 mm on three representative red-coated samples. A preliminary elemental spot-microanalysis was performed by SEM-EDS. After identifying a fairly homogenous area on each sample, point maps were drawn along an arbitrary line from the outer coating to the ceramic body in order to reveal possible compositional differences between the bodies and slips. The latter were also analysed by μ -Raman spectroscopy to investigate the presence and features of hematite. μ -Raman spectra (Leon et al., 2010; Lofrumento & Zoppi, 2004; Zoppi et al., 2006) were recorded using a single-grating Renishaw RM 2000 spectrometer equipped with an air-cooled device, coupled with a near-IR laser diode ($\lambda = 785$ nm). A 50x objective was used on a sample area of 1.5 μ m diameter, with incident laser power ranging from approximately 2 mW to 200 μ W for the diode, with varying acquisition times for each sample.

RESULTS

Ceramic bodies

All the samples present a fairly homogeneous texture and highly fine grained (depurated, as defined by many authors) body with small rounded and elongated pores with a preferential orientation parallel to the object walls. The colour of the body of the red-coated samples varies between soft red and pinkish, and the thickness does not exceed 5 mm, whereas it is about 1 cm in the moulds whose body is pinkish grey. Within the two main groups (coated ceramics and moulds), no subgroups could be distinguished macroscopically from the initial visual examination. Compared to the others, a coarser grain size was detected in sample CI-16 (red-coated), CI-17 (mould), and CI-18 (mould). On the basis of the petrographic features observed in thin sections (figure 1c), all samples are characterised by a fine-grained to very fine-grained body, well sorted and homogeneous texture with unimodal grain-size distribution. The abundance of inclusions is around 5% mainly composed by fine equant rounded quartz grains (≤ 50 μ m). All samples show a homogeneous and optically inactive matrix and a low porosity ($\leq 5\%$) composed of small spherical and elongated voids well-aligned with margins of sections. As already noted macroscopically, a coarser grain size was detected in samples CI-16, CI-17, and CI-18, with inclusions between 50 and 100 μ m in the first two and 100 and 200 μ m in CI-18. These samples also show polycrystalline quartz and plagioclase inclusions as well as a higher porosity composed of irregular and elongated voids (Figure 1c). In samples MP-2, PC-12, CI-18, and AT-23 microcrystals of secondary calcite are detected in some voids. The red slips appear to be homogeneous and well adherent to the body. In some cases, the presence of elongated voids at the interface between the coating and the ceramic body is observed (Figure 1c, sample MP-1).

Mineralogical composition

The mineralogical composition of ceramic bodies is very similar in all samples without distinction between moulds and coated ceramics. It includes both primary minerals as quartz, K-feldspar (microcline), illite/muscovite, and new phases formed during the firing process as hematite, diopside-like pyroxene, and plagioclase. In the case of such similar samples, of which the production centres and chronological frame are well known, the statistical treatment of diffraction data allows to simultaneously compare all the samples with the aim to identify similarities/differences among the various workshops, according to the different assemblage of the mineral phases. A cluster analysis of all raw XRPD data, using Euclidean distances and average linkage method, was performed to group the samples and evaluated according to the main parameters of the raw diffraction patterns, and in particular the position of the peaks. The dendrogram in Figure 2a shows the TSA samples grouped into five main clusters except PT-09, CI-18, AT-23, and AT-25, which do not group in any of them and can be considered outliers. Each cluster contains both matrices and coated ceramics, without any particular subdivision, regardless of the various workshops and the relative chronological period. Cluster analysis helped to select the most representative samples of each group (marked with an asterisk in Figure 2a) of which the relative diffractograms and microphotograph of the thin sections are shown in Figure 2b and c, respectively. It is important to consider that the clustering of samples is the result of a number of discriminant factors related to the mineralogical composition, such as the mineralogy and grain size of the used base clay, as well as the firing temperature, all acting together in defining the groups (Maritan et al., 2015). In particular, when the cluster analysis of XRPD data is performed on a set of ceramic samples that are very similar in terms of mineralogical composition and belonging to a specific area of production, it takes into account much finer differences that, as in this case, required an in-depth examination. The very fine-grained texture of the samples prevented the quantification of the mineralogical phases under the polarised-light microscope. Therefore, performing the Rietveld refinement was useful to assess this aspect, better highlighting the differences between the various clusters. The mineralogical assemblage of the 25 samples and the relative estimation of firing temperature is given in Table 2. The goodness of fit (GoF) and the weighted profile R-factor (Rwp) for each Rietveld refinement (Toby, 2006) are also reported. The results refer to the total of the mineral groups of plagioclases, K-feldspars, and pyroxenes, without specifying the intermediate phases of the solid solution. As for the plagioclase its main peak resulted to be very broad (see detail in Figure 2b sample MP-02, where the peak decomposition was highlighted) and was interpreted as the contribute of anorthite and albite-rich plagioclases. Because anorthite is unfrequently present in clays, its occurrence is related to the ceramic firing process of a carbonate-rich (calcareous) clay at temperature exceeding the decomposition of calcite ($>850^{\circ}\text{C}$ in oxidising conditions).

Chemical analysis

All the analysed ceramic bodies show a quite homogeneous chemical composition (as suggested by the low standard deviation values reported in Table 3) characterised by a high content of alkaline-earth elements ($\text{CaO} + \text{MgO} > 11\%$) and a moderately high concentration of iron (Fe_2O_3 7–8%), indicating the use of a carbonate- and iron-rich clay. All the TSA samples in the ternary system Al_2O_3 - $\text{CaO} + \text{MgO}$ - SiO_2 (Figure 3a) plot in the calcium-rich section just inside the stability field of silica-anorthite-pyroxene. As a matter of fact, the mineralogical composition of the studied samples is mainly given by quartz, plagioclases, and pyroxenes as the result of the complete reaction of the pristine fine-grained calcite with the phyllosilicates and quartz under complete equilibrium conditions (Heimann & Maggetti, 1981, 2019). Going back to the geochemistry, differences in the concentration of some elements are highlighted in the score and

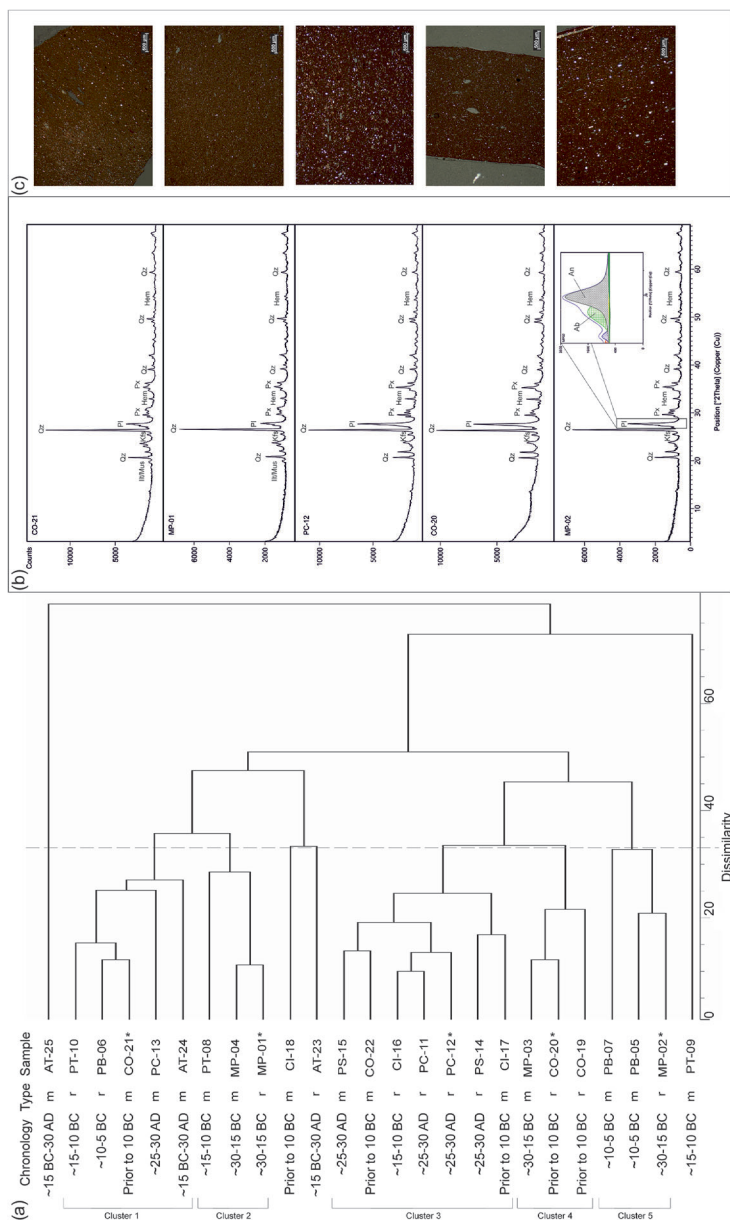


FIGURE 2 (a) Dendrogram obtained from the cluster analysis of XRPD patterns of TSA samples, according to Euclidean distance and average linkage method on position of peaks. Dissimilarity cut-off is based on KGS test. The most representative samples within each cluster are marked with an asterisk. (b) Diffraction patterns of the most representative samples of each cluster: CO-21 for Cluster 1, MP-01 for Cluster 2, PC-12 for Cluster 3, CO-20 for Cluster 4, MP-02 for Cluster 5. Abbreviation and type of the samples refer to Table 1. Mineral abbreviations according to Warr (2021): Qz = quartz, Pl = plagioclases, Px = pyroxenes, Hem = hematite, Ill/Mus = illite/muscovite. (c) Microphotographs of the thin sections of the most representative samples of each cluster (cross-polarised light).

TABLE 2 Results of the Rietveld refinement of XRPD data using the reference structure “silicabgm”. Rwp and GoF values from the refinement are reported. Abbreviations of the mineral phases according to Warr (2021): Qz = quartz, Pl = plagioclases, Px = pyroxenes, hem = hematite, Kfs = K-feldspar, Mus = muscovite. The estimation of the firing temperature (FT) is included.

Sample	Qz	Hem	Px	Pl	Kfs	Mus	Silicabgm	FT (°C)	Rwp	GoF
MP-01	18	4	6	14	7	5	44	900–950	7.93	2.12
MP-02	18	3	14	16	10	1	39	900–950	6.21	1.66
MP-03	15	3	12	15	8	1	44	900–950	6.25	1.73
MP-04	15	3	6	10	5	11	49	850–900	6.98	1.87
PB-05	16	3	15	16	8	1	40	900–950	6.35	1.59
PB-06	18	4	7	20	6	4	39	900–950	6.45	2.34
PB-07	16	7	8	34	9	3	22	900–950	6.56	2.33
PT-08	21	3	6	5	9	7	49	900–950	9.38	3.4
PT-09	20	1	4	2	6	6	61	900–950	8.15	2.92
PT-10	17	3	7	11	8	7	45	900–950	7.68	2.78
PC-11	10	2	8	14	6	1	57	900–950	6.36	2.27
PC-12	16	5	11	27	9	3	24	900–950	6.54	2.33
PC-13	25	3	7	23	12	3	25	900–950	6.47	2.32
PS-14	22	5	12	26	10	4	21	900–950	6.09	2.21
PS-15	12	4	6	21	6	2	49	900–950	6.88	2.53
CI-16	15	3	16	19	10	2	32	900–950	5.68	2.04
CI-17	18	3	15	21	12	3	26	900–950	5.56	2.01
CI-18	19	3	5	13	10	3	44	900–950	5.69	2.27
CO-19	9	3	6	17	5	1	57	900–950	6.51	2.48
CO-20	12	4	6	24	5	1	49	900–950	4.99	1.94
CO-21	15	2	6	15	6	4	52	900–950	6.59	2.42
CO-22	11	3	6	15	7	2	55	900–950	6.27	2.29
AT-23	18	2	19	15	10	5	28	900–950	5.15	2
AT-24	17	2	15	18	7	5	31	900–950	6.09	2.2
AT-25	4	1	13	23	3	/	56	950–1,000	7.05	2.67

loading plot of the principal components analysis (Figure 3b), which shows a random distribution of samples with no clear separation between moulds and red-coated wares, indicating the use of the same type of clay and clay preparation for the production of both types of object.

Chemical data of the studied samples were compared with that of the most important *terra sigillata* wares from regional and extraregional production centres. For this purpose, quantitative data of major, minor, and trace elements of *terra sigillata* from Italian territory: Arezzo (Tuscany region, central Italy) (Olcese & Picon, 2003), Pisa (Tuscany region, central Italy) (Schneider & Zabezhlicky-Scheffenegger, 2016), Padan area (Veneto region, northern Italy) (Maritan et al., 2013), Puteoli (today Pozzuoli, Campania region, southern Italy), Cales (today Caserta, Campania region, southern Italy) (Guarino et al., 2011) and the so-called “Produzione A della Baia di Napoli” (Campania region, southern Italy) (Grifa et al., 2019), and from abroad: Jaen, Malaga, and Mayorga (Spain) (Compana et al., 2014), Lyon (France) and Carthage (Tunisia) (Schindler-Kaudelka et al., 1997), northern and central Tunisia (Baklouti et al., 2015) and Turkey (Schneider & Zabezhlicky-Scheffenegger, 2016) were considered and statistically treated together with TSA samples here analysed. The statistical treatment was carried out, in this case, on a very small number of trace chemical elements, due to the structure of the

TABLE 3 Chemical composition of major, minor (expressed as oxide wt.%), and trace elements (expressed as ppm) of the studied samples. L.O.I. (loss on ignition), average and *SD* (standard deviation) are also reported.

	MP-02		MP-03		MP-04		PB-05		PB-06		PB-07		PT-09		PT-10		PC-11		PC-12		PC-13	
	Red-coated	Mould	Mould	Mould	Mould	Mould	Red-coated	Mould	Red-coated	Mould	Red-coated	Mould	Red-coated	Mould	Red-coated	Mould	Red-coated	Mould	Red-coated	Mould	Red-coated	Mould
SiO ₂	56.71	56.01	56.94	54.97	55.74	57.32	55.4	57.32	56.43	56.94	56.06	56.58	56.06	56.94	56.06	56.58	56.06	56.94	56.06	56.58	56.06	56.58
TiO ₂	0.9	0.92	0.95	0.91	0.97	0.87	0.93	0.87	0.9	0.9	0.89	0.89	0.9	0.9	0.89	0.89	0.9	0.9	0.89	0.89	0.89	0.89
Al ₂ O ₃	18.08	18.09	18.59	18.14	18.69	17.59	18.76	17.59	18.34	17.68	17.71	17.71	17.71	17.68	17.71	17.71	17.68	17.71	17.68	17.71	17.71	17.71
Fe ₂ O ₃	7.22	7.54	7.75	7.7	8.06	7.06	7.72	7.06	7.36	7.11	7.34	7.39	7.39	7.11	7.34	7.39	7.11	7.34	7.39	7.34	7.39	7.39
MnO	0.14	0.15	0.18	0.16	0.17	0.19	0.16	0.19	0.17	0.14	0.16	0.17	0.17	0.14	0.16	0.17	0.14	0.16	0.16	0.16	0.16	0.17
MgO	3.08	3.19	3.26	3.21	3.41	2.94	3.27	2.94	3.3	3.24	3.16	3.16	3.16	3.24	3.16	3.16	3.24	3.16	3.16	3.16	3.16	3.16
CaO	10.36	10.44	8.6	10.84	9.04	9.16	9.58	9.16	9.43	9.81	10.35	9.17	9.17	9.81	10.35	9.17	9.81	10.35	9.81	10.35	9.17	9.17
Na ₂ O	0.87	0.95	0.71	0.91	0.69	1.03	0.72	1.03	0.88	1	0.95	0.99	0.99	1	0.95	0.99	1	0.95	0.95	0.95	0.99	0.99
K ₂ O	2.45	2.41	2.55	2.44	2.49	2.7	2.41	2.7	2.73	2.41	2.36	2.5	2.5	2.41	2.36	2.5	2.41	2.36	2.36	2.36	2.5	2.5
P ₂ O ₅	0.25	0.26	0.27	0.27	0.26	0.34	0.23	0.34	0.28	0.25	0.24	0.9	0.9	0.25	0.24	0.9	0.25	0.24	0.24	0.24	0.9	0.9
Tot	100.06	99.96	99.8	99.55	99.52	99.2	99.18	99.2	99.82	99.48	99.22	99.46	99.46	99.48	99.22	99.46	99.48	99.22	99.22	99.22	99.46	99.46
L.O.I.	1.55	1.27	1.56	1.29	1.59	4.34	1.01	4.34	2.26	1.02	1.42	2.68	2.68	1.02	1.42	2.68	1.02	1.42	1.42	1.42	2.68	2.68
S	80	55	73	62	106	243	76	243	196	79	82	161	161	79	82	161	79	82	82	82	161	161
Sc	20	23	19	22	19	18	21	18	19	19	21	19	19	18	21	19	19	21	21	21	19	19
V	136	111	140	127	137	137	141	137	140	130	130	113	113	130	130	113	130	130	130	130	113	113
Cr	162	167	171	170	180	144	175	144	179	170	164	167	167	170	164	167	170	164	164	164	167	167
Co	25	29	23	24	26	27	27	27	25	24	26	27	27	25	24	27	25	24	24	24	26	27
Ni	86	91	95	91	98	93	94	93	96	88	89	92	92	96	88	92	96	88	88	89	92	92
Cu	61	51	47	54	54	43	47	43	45	53	46	52	52	43	46	52	45	53	46	46	52	52
Zn	125	133	140	136	142	109	135	109	125	133	130	139	139	109	133	139	125	133	130	130	139	139
Ga	14	12	15	13	15	11	16	11	15	13	14	15	15	11	13	15	15	13	14	14	15	15
Rb	120	117	135	124	131	136	130	136	141	120	125	126	126	136	120	126	141	120	125	125	126	126
Sr	298	316	265	330	271	279	276	279	288	303	285	297	297	279	303	297	288	303	285	285	297	297
Y	25	25	29	26	27	25	30	27	27	26	27	27	27	25	26	27	27	26	26	27	27	27
Zr	144	148	139	149	140	156	132	156	149	158	150	152	152	156	158	152	149	158	158	150	152	152
Nb	21	21	22	20	25	20	23	20	22	21	17	20	20	20	21	20	22	21	17	17	20	20

TABLE 3 (Continued)

	MP-02	MP-03	MP-04	PB-05	PB-06	PB-07	PT-09	PT-10	PC-11	PC-12	PC-13
Ba	431	448	436	416	436	415	569	460	394	398	563
La	38	30	36	33	38	42	38	37	36	39	32
Ce	82	70	80	74	81	88	81	80	78	82	70
Nd	33	37	36	36	41	43	31	35	34	36	31
Pb	27	31	31	29	28	28	30	28	28	23	28
Th	16	15	17	16	19	17	15	16	16	16	15
U	2	4	3	3	2	2	4	3	4	5	3

TABLE 3 (Continued)

	PS-14		PS-15		CI-16		CI-17		CI-18		CO-19		CO-20		CO-21		CO-22		AT-23		AT-24		AT-25		Media	S.D.
	Red-coated	Mould	Red-coated	Mould	Red-coated	Mould	Red-coated	Mould	Red-coated	Mould	Red-coated	Mould	Red-coated	Mould	Red-coated	Mould	Red-coated	Mould	Red-coated	Mould	Red-coated	Mould	Red-coated	Mould		
SiO2	56.59	55.24	54.27	54.42	58.74	55.02	56.11	57.16	55.01	54.16	53.97	53.57	55.80	1.27												
TiO2	0.94	0.98	0.9	0.92	0.89	0.98	0.93	0.93	0.98	0.97	0.91	0.89	0.92	0.03												
Al2O3	18.72	19.02	18.06	17.98	17.34	19.47	18.69	18.47	18.82	18.17	17.45	17.63	18.23	0.56												
Fe2O3	7.66	8.07	7.67	7.78	7.47	7.78	7.56	7.53	8.1	8.33	7.49	7.48	7.62	0.32												
MnO	0.16	0.16	0.2	0.2	0.19	0.17	0.15	0.15	0.18	0.15	0.14	0.15	0.16	0.02												
MgO	3.31	3.47	3.36	3.34	3.15	3.63	3.27	3.35	3.72	3.01	3.18	3.16	3.27	0.18												
CaO	9.37	9.57	11.29	10.49	7.63	9.99	9.59	8.35	9.23	11.86	12.63	13.05	9.99	1.30												
Na2O	0.87	0.8	0.91	0.93	1.25	0.87	0.83	0.85	0.9	0.8	0.8	0.89	0.89	0.12												
K2O	2.55	2.25	2.39	2.46	2.56	2.35	2.46	2.76	2.43	2.39	2.44	2.19	2.46	0.14												
P2O5	0.27	0.25	0.28	0.5	0.4	0.31	0.23	0.26	0.44	0.3	0.26	0.25	0.32	0.14												
Tot	100.44	99.81	99.33	99.02	99.62	100.57	99.82	99.81	99.81	100.14	99.27	99.26	99.66	0.41												
L.O.I.	1.03	1.41	1.94	2.26	2.28	1.59	1.34	2.14	1.89	1.98	3.64	1.18	1.86	0.82												
S	70	106	150	182	91	48	76	104	39	198	295	29	113.09	69.20												
Sc	21	19	22	21	17	24	19	20	20	26	25	25	20.83	2.41												
V	133	132	125	112	104	121	138	122	123	129	118	133	127.48	10.48												
Cr	176	184	168	177	176	190	169	174	194	181	162	176	172.87	10.33												
Co	27	29	26	24	24	30	26	26	28	24	28	23	26.00	1.98												

TABLE 3 (Continued)

	PS-14	PS-15	CI-16	CI-17	CI-18	CO-19	CO-20	CO-21	CO-22	AT-23	AT-24	AT-25	Media	S.D.
Ni	95	105	95	100	97	105	90	96	108	96	107	91	95.57	
Cu	46	54	44	43	34	56	49	53	48	49	45	42	48.52	5.79
Zn	136	147	125	121	117	136	131	156	140	141	128	129	132.78	10.13
Ga	14	15	14	13	12	13	15	14	15	12	12	13	13.70	1.33
Rb	128	121	116	123	119	112	131	140	113	113	125	114	124.35	8.61
Sr	279	287	319	312	256	301	278	271	280	357	347	348	297.52	27.82
Y	27	30	25	28	26	30	28	27	28	30	26	26	27.17	1.70
Zr	141	135	152	156	177	157	135	150	157	151	144	142	148.43	9.85
Nb	21	23	20	22	18	23	21	20	21	23	22	19	21.09	1.78
Ba	429	411	454	489	500	431	407	445	486	438	399	383	445.13	48.72
La	42	44	43	41	31	46	34	37	35	40	38	30	37.39	4.45
Ce	91	89	89	82	70	95	78	80	77	85	83	70	80.65	6.95
Nd	37	39	35	37	36	42	39	40	40	34	39	34	36.74	3.25
Pb	30	28	32	29	39	29	23	45	41	27	27	25	29.83	5.26
Th	19	17	17	17	17	20	15	17	18	17	18	17	16.83	1.34
U	5	3	2	2	5	5	3	2	5	4	3	2	3.30	1.15

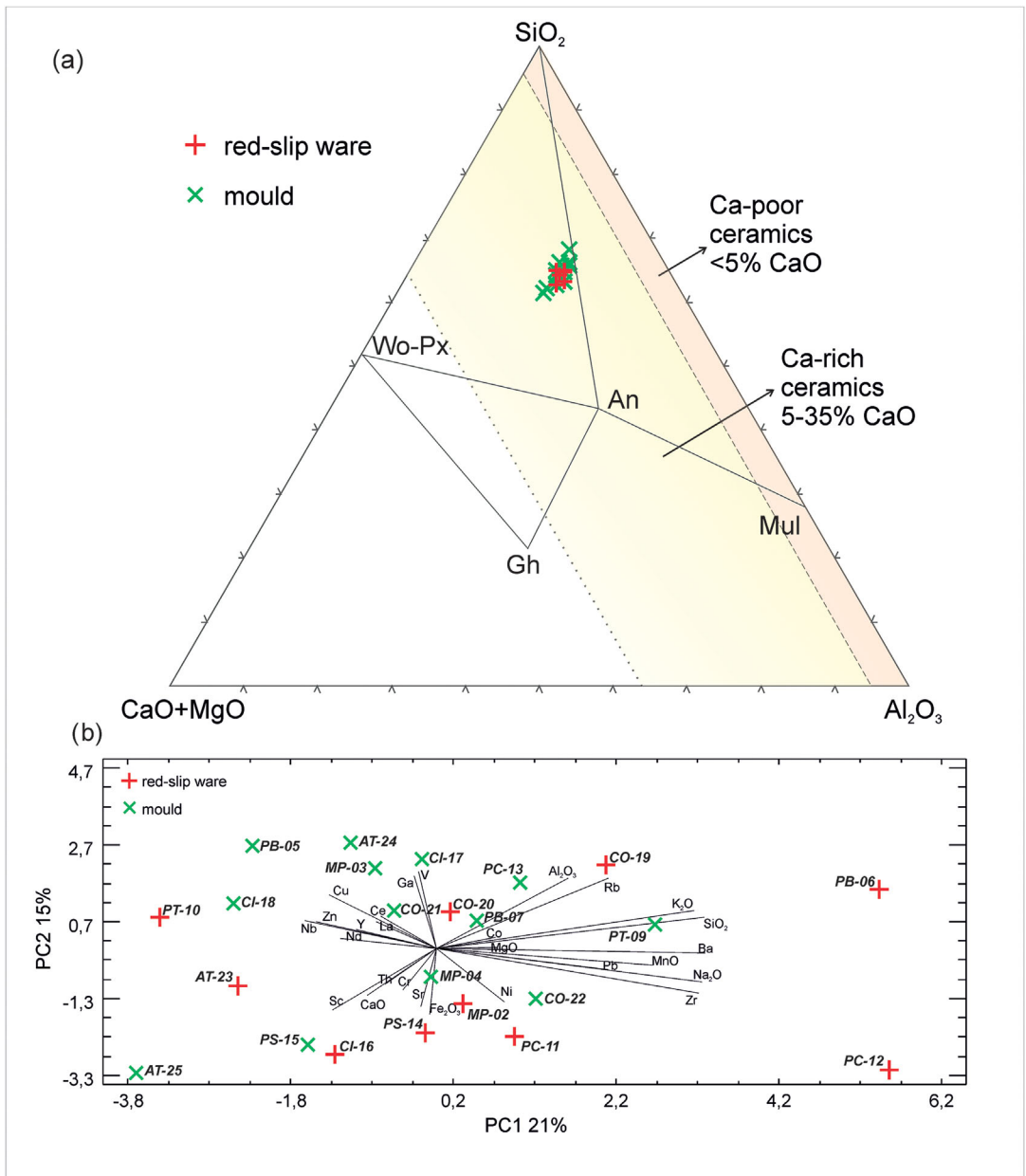


FIGURE 3 (a) SiO_2 - Al_2O_3 - CaO ternary diagram with mineral stability fields (Wo: wollastonite; Gh: gehlenite; An: anorthite, Mul: mullite), reporting the plot of the composition of the TSA samples. Field of Ca-poor and Ca-rich clay are also reported with shades of orange and yellow, respectively. (b) Score and loading plot of principal component analysis performed on a log-transformed subset of elements (excluding S, U, P_2O_5 for their high ratio between total variation (vt) and variance(t) divided by TiO_2). PC1, and PC2 represent 21% and 15% of the total variance respectively.

database for which only elements common to all the studies were considered. The homogeneity in chemical composition is also confirmed by the score plot of the principal component analysis (Figure 4), which clearly shows how all the TSA samples completely overlap with those from Arezzo, already analysed in previous studies (Olcese & Picon, 2003), and show a very high

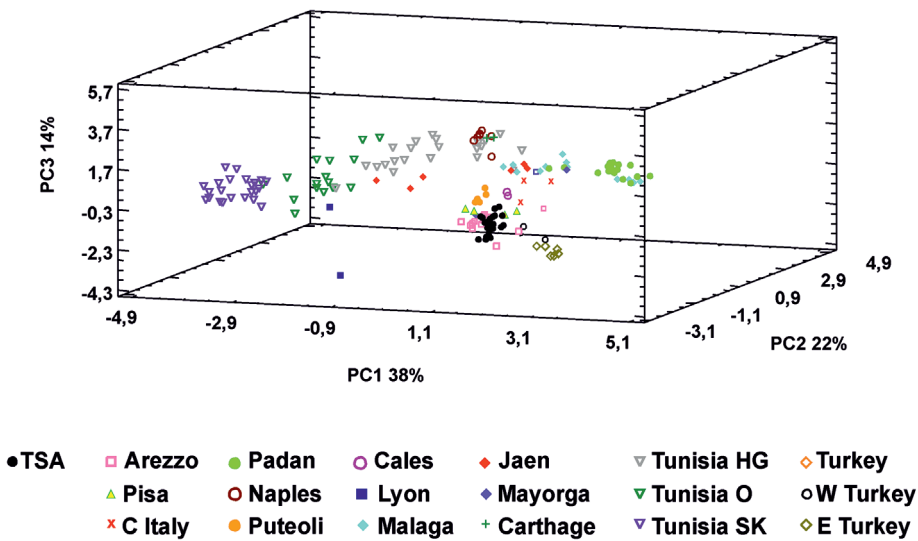


FIGURE 4 Score plot of the principal component analysis performed on a log-transformed subset of elements (SiO_2 , TiO_2 , Al_2O_3 , Fe_2O_3 , MnO , MgO , CaO , Na_2O , K_2O , P_2O_5 , Ni , Rb , Sr , Y , Zr) divided by TiO_2 , with PC1, PC2, and PC3, representing 38%, 22% and 14% of the total variance, respectively.

chemical affinity with those from Pisa. They result also chemically close to the *terra sigillata* from Puteoli and Cales.

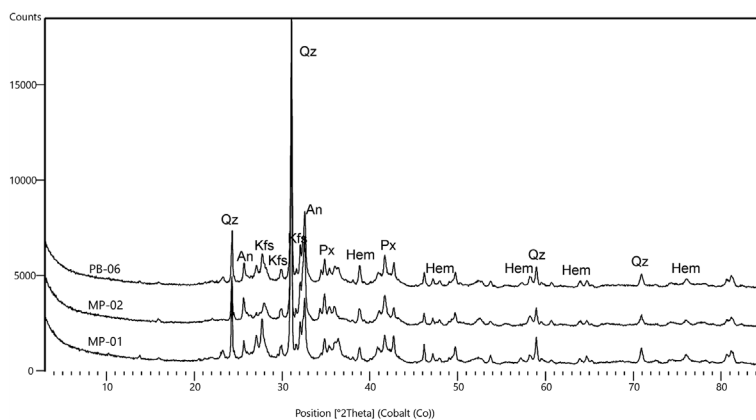
Red slips

The coating appears isotropic, compact, and well adherent to the ceramic body in all samples, and its thickness varies from approximately 20 to 40 μm (Figure 1c-d). Under the SEM, the red slips show a glassy matrix where micrometric grains of quartz and nanometric crystals with a higher average atomic number are embedded (Figure 1d). The latter could not be precisely analysed because their size is much lower than the spot beam. A preliminary SEM-EDS spot microanalysis was carried out on samples MP-01, MP-02, and PB-06, selected as representative for the good quality of the coating. The results reported in Table 4 showed substantial differences in the concentration of some elements between the bodies and the red slips. In particular, there is a higher concentration of aluminium and a dramatic decrease of calcium in the coatings, where the potassium content is about twice the level found in the bodies. Iron is also higher in the coatings, except in sample PB-06. The diffraction patterns of that three red-coated samples are reported in Figure 5 and indicate the presence of hematite, anorthite and pyroxenes (diopside-like) as phases formed during firing. Quartz and K-feldspar are present as primary phases. The μ -Raman spectroscopy analysis of the red slips was performed on all 10 coated samples to investigate the hematite, even if, in sigillata red slips, it is not the predominant phase but usually displays the most intense spectrum overwhelming the other phases (Sciau et al., 2020).

Figure 6a shows the acquired Raman spectra of the red slips that were compared to those of pure hematite and hematite with a substitution of aluminium content of 8% (Figure 6b). A multiplex fitting analysis, using a mixed Gaussian-Lorentzian function and a quadratic basis function, was employed to estimate peak positions and widths averaged over five measurements for each sample. The results revealed broader peaks shifted to higher wavenumbers (Figure 6b) compared to those of pure hematite (α - Fe_2O_3). This observation aligns with a disordered phase

TABLE 4 Elemental composition of slips and bodies of three selected samples by SEM-EDS spot microanalysis (oxides concentration normalized to 100%); bdl = below detection limit.

Sample	Layer	Al ₂ O ₃	SiO ₂	Fe ₂ O ₃	K ₂ O	MgO	CaO	TiO ₂	Na ₂ O
MP-01	Slip	22.57	49.91	13.33	7.64	3.87	2.04	0.63	Bdl
	Ceramic body	16.10	51.25	11.29	3.32	3.60	13.36	1.09	Bdl
MP-02	Slip	31.23	30.43	20.56	6.42	7.80	2.58	0.97	Bdl
	Ceramic body	14.55	48.65	13.31	3.26	3.25	16.00	1.07	Bdl
PB-06	Slip	27.30	42.01	14.85	6.50	5.49	1.99	0.79	1.07
	Ceramic body	14.28	32.39	35.77	2.13	5.57	8.53	1.33	Bdl

**FIGURE 5** Diffraction patterns of the slip of samples MP-01, MP-02, and PB-06 showing the same mineralogical assemblage. Mineral abbreviations according to Warr (2021): Qz = quartz, an = anorthite, Px = pyroxenes, hem = hematite, Kfs = K-feldspar.

indicating aluminium substitution in the haematite lattice, which is also reflected by the occurrence of a high frequency band located near 670 cm^{-1} and a right shoulder of the band at 412 cm^{-1} , close to 430 cm^{-1} . Because this region is quite sensitive to the geometry of FeO_6 octahedra, being the 412 cm^{-1} signal attributed to O-Fe-O bending mode, this additional band could be related to a local distortion caused by Al ions. The contribution of the 670 cm^{-1} band is further indicated by the height ratio $670/612$. Therefore, the fitting results are consistent with hematite featuring approximately 8% aluminium substitution (Zoppi et al., 2006, 2008).

DISCUSSION

Macro- and microscopic observation of the ceramic bodies show that there are no clear differences between matrices and coated wares nor between the samples attributed to the various workshops. Thin-section textural analysis revealed a very fine grain size of inclusions with strongly unimodal distribution that can be the result of an intentional depuration process (or the use of a very fine-grained clayey material), as well as the low porosity detected in all samples (Quinn, 2022). An exception is represented by three samples found in Cincelli site (CI-16, a red-coated sample sealed by *Tigranus*, and CI-17 and CI-18, fragments of moulds where no stamps were identified) showing larger grain size of inclusions and a higher presence of voids with respect to the others. The other fragments (CO-19, CO-20, CO-21) coming from this site

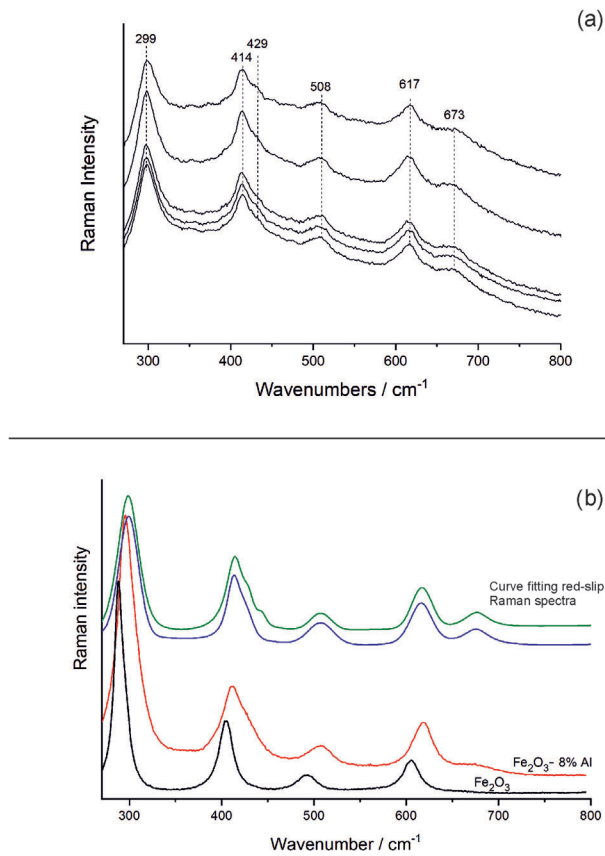


FIGURE 6 (a) Typical Raman spectra of the samples of the sigillata red slip. (b) Curve fitting of red-slip Raman spectra (top), pure hematite and Al-substituted hematite (bottom).

and attributed to *Cornelius* (Table 1) do not show the same textural characteristics. Having no information regarding the attribution of samples CI-17 and CI-18, it is not possible to draw conclusions regarding the potential correlation between the textural and granulometric characteristics of these samples with a specific workshop, but it would certainly be interesting to investigate this further. The deliberate refining of clay by artisans can be difficult to detect in thin sections, and it is not always possible to know exactly what type of refining method (sieving, settling, or levigation) was used by potters. However, considering the similar composition showed by mineralogical and chemical analysis, is plausible to hypothesise a difference in the refinement process rather than a different clay source. The mineralogical associations detected by XRPD analysis indicate that all samples were produced from calcareous-illitic clay material. The presence of pyroxene in all samples constrains the firing temperature above those of the decomposition of calcite, therefore exceeding 850°C. Calcite reacts with silica and phyllosilicates (or their product of decomposition) forming pyroxene (calcium–magnesium silicate such as diopside) and anorthite at temperatures above 850°C (Grammatikakis et al., 2019; Trindade et al., 2009). What emerges from the mineralogical analysis (Table 2) is that the proportion of muscovite/illite phase to pyroxenes and plagioclases could be considered as one of the main discriminator factor between the various samples. With reference to several results reported on the thermal behaviour of illitic raw clay (Crespo-López & Cultrone, 2022; Khalfaoui & Hajjaji, 2009; Mazzucato et al., 1999; Pérez-Monserrat et al., 2022), the illite/muscovite phase persists up to 950°C, after which it completely decomposes. The results suggest

that a dehydroxylation process of illite/muscovite occurs between 800°C and 1000°C, leading to the development of the high-temperature phase. Therefore, it was possible to identify illite/muscovite (muscovite-2 M) peaks by XRPD analysis even in association with high-temperature phases such as diopside-like pyroxenes. Microstructural observation at SEM was a useful tool to confirm the co-presence of these mineral phases, as shown in Figure 1d, where muscovite crystals in the process of thermal breakdown are recognisable. In the majority of samples, the mineralogical phases representing the residual component of the base clay, such as illite/muscovite, quartz, and K-feldspar, together with calcium and aluminium silicates, (anorthite-rich plagioclases and diopside) as neoformation mineral phases due to the firing process, and hematite, suggest a heating temperature between 900°C and 950°C (Maritan et al., 2006; Nodari et al., 2007). Based on the considerations made so far, the mineralogical associations of sample MP-04 suggest a lower firing temperature not exceeding 900°C, whereas in sample AT-25 the higher amount of pyroxene and plagioclases together with the scarce presence of quartz and the absence of muscovite phase, indicate a temperature between 950°C and 1000°C. Considering the level of similarity among the studied samples, some differences in firing temperature can be interpreted as the result of a more or less long time of residence in the kiln or to an inhomogeneous heat distribution within the kiln due to the density of the objects inside the firing chamber rather than a different heating process.

Under a geochemical point of view, the results of the principal component analysis (Figure 3b) clearly indicate that, despite some divergences mainly due to the different concentration of some elements, no specific groups are formed, neither by type nor in regard to samples from the same workshop. This is related to the use of a common base clays (probably different levels of the same deposits) and a very similar degree of depuration to obtain the clay paste for producing both moulds and red-coated ware. Looking at the chemical composition (Table 3) the samples attributed to *Ateius* workshop (AT-23, AT-24, and AT-25) show the highest CaO content, confirming what already emerged in Schneider and Hoffmann (1990) and Schneider and Zabehllicky-Scheffenecker (2016).

Chemical data of TSA samples, here studied, fairly matched those from the other main productions of central Italy (Figure 4), first and foremost that of Pisa, where kiln discharges were found mainly attributable to the manufacturing activities of *Ateius* and his artisans. Regional similarities can be the result of geological factors, which cause clays with similar compositions to be found in many parts of the same region (Tuscany, in this case). However, human factors play an important role in this similarity, and the proliferation of products with analogous compositions can also be explained by the fact that when a particular clay showed specific qualities, potters tried to find deposits of it in other parts of the region (Cuomo di Caprio & Picon, 1994). Compositional affinities can be individuated also with the Puteolan and Calenian samples, for which a high-CaO clay deposit was used (Grifa et al., 2019; Guarino et al., 2011). The discrete similarity between these groups suggests a specific selection of raw material for the *terra sigillata* ware production oriented to the choice of Ca-rich clays. It is already known that the thermal behaviour of carbonate-rich clays has technological advantages for both the firing of the ceramic body and the coating (Sciau et al., 2020). The sintering process is promoted at lower temperatures than in noncarbonate clays (around 800°C) due to the presence of melting agents such as Mg and Ca, making the work of ancient potters easier and less energy consuming (Heimann & Maggetti, 2019; Trindade et al., 2009). For what concerns the slips, the presence of aluminium in the crystal lattice of hematite, resulting in a change in the relative lattice vibrations in the Raman spectra, is related to the crystallization of the iron oxide in a system very rich in aluminium, such as that provided by a very depurated clay (enriched in phyllosilicates and iron oxides). The Al enrichment is also evident from SEM-EDS analysis, which shows an aluminium content around 20–30% in the slips. The high Mg content is consistent with what has already been experienced in other studies on *Italic terra sigillata* (Leon et al., 2015) in comparison with the French production showing low concentration of magnesium in the slips and

higher firing temperature. The presence of magnesium plays an important role in the quality and microstructure of the coatings. Magnesium and calcium silicates (pyroxenes), which are formed by the reaction of carbonates between 850 and 900°C, improve the mechanical properties of the coatings by increasing compressive strength and reducing crack formation (Pradell & Molera, 2020). Moreover, a magnesium concentration of more than 3% in the slips may be related to the possible formation of spinel nanocrystals, derived from the decomposition of illite, which acts as a melting agent favouring the vitrification process at temperature below 1000°C. The frequency bands near 670 cm⁻¹ and 412 cm⁻¹ (Figure 6) could be markers for the presence of spinel phases associated with haematite in the coatings, although these are only preliminary data that should be studied further. Another interesting result is the enrichment of potassium in the coatings, a factor that could be decisive in the quality of the final product. During firing, potassium compounds function as fluxes, facilitating the sintering process and the surface clay's consequent vitrification (Mirti et al., 1999). The high potassium content is related to the presence of a higher concentration of illite/muscovite in the clay used for the slip than in that used for the ceramic body, as the result of a more effective depuration process in which the concentrated phyllosilicate and other mineral phases (especially carbonates) were separated. The high petrographic and chemical homogeneity of the studied samples suggests the use of a raw material extracted from the same clay deposit. Although this contribution does not focus on questions of provenance, as the material studied was locally produced, some general considerations are given below. The geographic vicinity of the main known production centres of *terra sigillata* in Arezzo, as well as their moderately calcareous composition, indicate that the Plio-Pleistocene sedimentary deposit of the Arezzo–Quarata clay formations (Peña & Gallimore, 2014; Peña & Blackman, 1994; relevant sheet of the Carta geologica d'Italia, foglio 114) was exploited for this ceramic production. Clayey outcrops enriched in the fluvial sandy and arenaceous components typical of the area near the right bank of the Arno River were also indicated as possible georesources. Considering the differences in the chemical composition of the coatings compared to the ceramic bodies, especially with regard to Ca content (Table 4), it is reasonable to assume that clays obtained from two different parts of the Arezzo–Quarata formation were used. Even if there are still uncertainties about the organisation of production process, the studies made so far on the basis of the findings of remains of kilns and clay purification tanks (Corchia & Zaccagnino, 2005) could suggest the presence of a few main workshops located in strategic positions and numerous smaller sites that functioned as operational branches of the bigger ones. It is also assumed that the main workshops supplied the small ones with selected, already purified clay, which they then either used for firing in their kilns or returned the semiprocessed product that was fired in the main facilities (Pucci, 1973). Bearing in mind that these are hypotheses that would require further investigation, this system could explain the homogeneous quality of the final products as well as the presence of selected craftsmen able to operate in specific steps of the production process. Previous studies (Widemann et al., 1975) have also hypothesised the employment of skilled craftsmen and equipment from Arezzo in Ateius' workshop branches in France.

CONCLUSION

The archaeometric analysis of mould and red-coated *terra sigillata* sherds found in Arezzo indicates a very standardized production technology over a period ranging between the ~30–15 BCE and the ~25–30 CE. The almost uniform chemical composition of the ceramic bodies clearly indicated that, despite the objects were produced in different workshops, the same carbonate-rich illitic base clay with a very similar degree of depuration was used. The raw clay material was probably sourced from specific outcrops of the Arezzo–Quarata clay formation, in the area along the banks of the Arno, not far from where the remains of Cincelli's workshops

were found. As for the slips, the use of a K-rich and Fe-rich illitic clay with a relatively low CaO content is suggested. Moreover, the range of firing temperature, determined on a mineralogical base, suggest a unified firing technology, which leads to the hypothesis of the use of the same type of kiln and firing in terms of quantity of fuel, the drought of the kiln, and length of the entire firing process. The results of this work indicate that, from *Marcus Perennius* onward, highly experienced potters working in the same workshops in Arezzo used a common recipe for the production of *terra sigillata* ware.

ACKNOWLEDGEMENTS

The authors would like to thank the National Archaeological Museum of Arezzo for providing the ceramic samples investigated in this paper. The fragments of *terra sigillata*, from the Museum's deposits, were made available in 2014 for the realisation of a master thesis, from which the present work originated. They are also grateful to Daria Pasqual and Jacopo Nava of the University of Padova for their collaboration in XRF, and SEM imaging respectively, to Marco Favero for the XRPD analysis and to Stefano Castelli for the photographs of the ceramic fragments. Open access publishing facilitated by Università degli Studi di Padova, as part of the Wiley - CRUI-CARE agreement.

DATA AVAILABILITY STATEMENT

The data that supports the findings of this study are all included within this article.

ORCID

Maria Emanuela Mascaro  <https://orcid.org/0000-0002-5788-3567>

Emma Cantisani  <https://orcid.org/0000-0002-4909-5624>

Marilena Ricci  <https://orcid.org/0000-0001-7894-7737>

Maria Chiara Dalconi  <https://orcid.org/0000-0001-8271-8929>

Lara Maritan  <https://orcid.org/0000-0002-3796-1265>

REFERENCES

- Aquilia, E., Barone, G., Mazzoleni, P., Raneri, S., & Lamagna, G. (2015). Petro-archaeometric characterization of potteries from a kiln in Adrano, Sicily. *Heritage Science*, 3, 11. <https://doi.org/10.1186/s40494-015-0043-4>
- Baklouti, S., Maritan, L., Laridhi Ouazaa, N., Mazzoli, C., Larabi Kassaa, S., Joron, J.-L., Fouzaï, B., Casas Duocastella, L., & Labayed-Lahdari, M. (2015). African terra sigillata from Henchir Es-Srira archaeological site, Central Tunisia: Archaeological provenance and raw materials based on chemical analysis. *Applied Clay Science*, 105–106, 27–40. <https://doi.org/10.1016/j.clay.2014.12.020>
- Baxter, M. J. (1999). Detecting multivariate outliers in artefact compositional data. *Archaeometry*, 41, 321–338. <https://doi.org/10.1111/j.1475-4754.1999.tb00986.x>
- Baxter, M. J. (2006). A review of supervised and unsupervised pattern recognition in archaeometry. *Archaeometry*, 48, 671–694.
- Brando M. (2008). Samia Vasa, i Vasi “di Samo”. In F. Filippi, *Horti et Sordes, uno scavo alle falde del Gianicolo*, Quasar, Roma (pp.127-174).
- Buxeda i Garrigós, J. (1999). Alteration and contamination of archaeological ceramics: the perturbation problem. *Journal of Archaeological Science*, 26, 295-313. <https://doi.org/10.1006/jasc.1998.0390>
- Carta geologica d'Italia, foglio 114, pp. 127–174. <https://sgi.isprambiente.it/geologia100k/>
- Compana, J. M., Cabeza, A., Aranda, M. A. G., & León-Reina, L. (2014). The Baetican workshops: A starting point to study Terra Sigillata Hispanica. *Journal of Archaeological Science*, 45, 26–35. <https://doi.org/10.1016/j.jas.2014.01.003>
- Corchia, R., & Zaccagnino, C. (2005). Una villa Romana a Cincelli (Arezzo). *Archeologia Classica*, 56, 557–579. <http://www.jstor.org/stable/44367674>
- Crespo-López, L., & Cultrone, G. (2022). Improvement in the petrophysical properties of solid bricks by adding household glass waste. *Journal of Building Engineering*, 59, 105039. <https://doi.org/10.1016/j.job.2022.105039>
- Cuomo Di Caprio, C., & Picon, M. (1994). Classification et détermination d'origine des céramiques à vernis noir et à vernis rouge d'Italie: aspects méthodologiques. In F. Burrigato, O. Grubessi, & L. Lazzarini *Proceedings of the 1st European workshop on archaeological ceramics*. Università degli Studi di Roma, Roma, p. 163-181.
- De La Torre, A. G., Bruque, S., & Aranda, M. A. G. (2001). Rietveld quantitative amorphous content analysis. *Journal of Applied Crystallography*, 34, 196–202. <https://doi.org/10.1107/S0021889801002485>

- Döbelin, N., & Kleeberg, R. (2015). Profex: A graphical user interface for the Rietveld refinement program BGMN. *Journal of Applied Crystallography*, *48*, 1573–1580. <https://doi.org/10.1107/S1600576715014685>
- Grammatikakis, E., Kyriakidis, Demadis, D., Diaz, C., & Leon-Reina, L. (2019). Mineralogical characterization and firing temperature delineation on Minoan pottery, focusing on the application of Micro-Raman spectroscopy. *Heritage*, *2*, 2652–2664. <https://doi.org/10.3390/heritage2030163>
- Grifa, C., Germinario, C., De Bonis, A., Langella, A., Mercurio, M., Izzo, F., Smiljanic, D., Guarino, V., Di Mauro, S., & Soricelli, G. (2019). Comparing ceramic technologies: The production of Terra Sigillata in Puteoli and in the bay of Naples. *Journal of Archaeological Science: Reports*, *23*, 291–303. <https://doi.org/10.1016/j.jasrep.2018.10.014>
- Guarino, V., De Bonis, A., Grifa, C., Langella, A., Morra, V., & Pedroni, L. (2011). Archaeometric Study on Terra Sigillata from Cales (Italy). *80*. <https://doi.org/10.2451/2011PMP0030>
- Guerrini, C., & Mancini, L. (2007). La ceramica di età romana. In *Introduzione Allo Studio Della Ceramica in Archeologia*. Dipartimento di Archeologia e Storia delle Arti, Università di Siena, Edizione: Centro Editoriale Toscano sas – Firenze (pp. 197–234).
- Heimann, R. B., & Maggetti, M. (1981). Experiments on simulated burial of calcareous terra sigillata (mineralogical change). Preliminary results. *Scientific Studies in Ancient Ceramics*, *19*, 163–177.
- Heimann, R. B., & Maggetti, M. (2019). The struggle between thermodynamics and kinetics: Phase evolution of ancient and historical ceramics. In *The contribution of mineralogy to cultural heritage* (pp. 233–282). Mineralogical Society of Great Britain and Ireland. <https://doi.org/10.1180/EMU-notes.20.6>
- Kelley, L. A., Gardner, S. P., & Sutcliffe, M. J. (1996). An automated approach for clustering an ensemble of NMR-derived protein structures into conformationally-related subfamilies. *Protein Engineering*, *9*, 1063–1065. <https://doi.org/10.1093/protein/9.11.1063>
- Khalifaoui, A., & Hajjaji, M. (2009). A Chloritic-illitic clay from Morocco: Temperature–time–transformation and neoformation. *Applied Clay Science*, *45*, 83–89. <https://doi.org/10.1016/j.clay.2009.03.006>
- Leon, Y., Lofrumento, C., Zoppi, A., Carles, R., Castellucci, E. M., & Sciau, P. (2010). Micro-Raman investigation of terra sigillata slips: A comparative study of central Italian and southern Gaul productions: Micro-Raman investigation of terra sigillata slips from Italy and Gaul. *Journal of Raman Spectroscopy*, *41*, 1550–1555. <https://doi.org/10.1002/jrs.2678>
- Leon, Y., Sciau, P., Passelac, M., Sanchez, C., Sablayrolles, R., Goudeau, P., & Tamura, N. (2015). Evolution of terra sigillata technology from Italy to Gaul through a multi-technique approach. *Journal of Analytical Atomic Spectrometry*, *30*, 658–665. <https://doi.org/10.1039/C4JA00367E>
- Lofrumento, C., & Zoppi, A. (2004). Micro-Raman spectroscopy of ancient ceramics: A study of French sigillata wares. *Journal of Raman Spectroscopy*, *35*, 650–655. <https://doi.org/10.1002/jrs.1209>
- Madsen, I., Scarlett, N., & Kern, A. (2011). Description and survey of methodologies for the determination of amorphous content via X-ray powder diffraction. *Zeitschrift Für Kristallographie*, *226*, 944–955. <https://doi.org/10.1524/zkri.2011.1437>
- Maritan, L. (2024). Ceramics: Chemical and petrographic analysis. In E. Nikita & T. Rehren (Eds.), *Encyclopedia of archaeology* (Vol. 2B) (pp. 386–397). Academic Press. <https://doi.org/10.1016/B978-0-323-90799-6.00020-3>
- Maritan, L., Holakooei, P., & Mazzoli, C. (2015). Cluster analysis of XRPD data in ancient ceramics: What for? *Applied Clay Science*, *114*, 540–549. <https://doi.org/10.1016/j.clay.2015.07.016>
- Maritan, L., Nodari, L., Mazzoli, C., Milano, A., & Russo, U. (2006). Influence of firing conditions on ceramic products: Experimental study on clay rich in organic matter. *Applied Clay Science*, *31*, 1–15. <https://doi.org/10.1016/j.clay.2005.08.007>
- Maritan, L., Secco, M., Mazzoli, C., Mantovani, V., & Bonetto, J. (2013). The decorated Padan terra sigillata from the site of Retratto, Adria (North-Eastern Italy): Provenance and production technology. *Applied Clay Science*, *82*, 62–69. <https://doi.org/10.1016/j.clay.2013.05.020>
- Mazzucato, E., Artioli, G., & Gualtieri, A. (1999). High temperature dehydroxylation of muscovite 2M1: A kinetic study by in situ XRPD. *Physics and Chemistry of Minerals*, *26*, 375–381. <https://doi.org/10.1007/s002690050197>
- Menchelli, S. (2005). La terra sigillata. In D. Gandolfi *La ceramica e i materiali di età romana. Classi, produzioni, commerci e consumi*, Bordighera, (pp. 155–168).
- Mirti, P., Appolonia, L., & Casoli, A. (1999). Technological features of Roman Terra Sigillata from Gallic and Italian Centres of production. *Journal of Archaeological Science*, *26*(12), 1427–1435. <https://doi.org/10.1006/jasc.1999.0435>
- Morel, J. P. (2009). Le produzioni ceramiche a vernice nera di Arezzo. In *Arezzo nell'antichità* (pp. 125–134). Giorgio Bretschneider Editore.
- Nodari, L., Marcuz, E., Maritan, L., Mazzoli, C., & Russo, U. (2007). Hematite nucleation and growth in the firing of carbonate-rich clay for pottery production. *Journal of the European Ceramic Society*, *27*, 4665–4673. <https://doi.org/10.1016/j.jeurceramsoc.2007.03.031>
- Olcese, G., & Picon, M. (2003). Terra Sigillata Italica a Roma e in area romana: Produzione, circolazione e analisi di laboratorio. *RCRF Acta*, *38*, 11–26.
- Peña, J. T., & Blackman, M. J. (1994). A neutron activation study of Plio-Pleistocene marine clays from west Central Italy: Compositional variability and implications for the proveniencing of Italian fineware pottery. In F.

- Burrigato, O. Grubessi and L. Lazzarini, *First European Workshop on Archaeological Ceramics* Università di Roma, (pp. 313–321).
- Peña, J. T., & Gallimore, S. (2014). Black-gloss ware, north Etrurian red-slip ware, and Italian Terra Sigillata from Cetamura Del chianti: Composition, provenance, supply, and consumption. *HEROM - Journal on Hellenistic and Roman Material Culture.*, 3, 71–224. <https://doi.org/10.11116/HEROM.3.4>
- Pérez-Monserrat, E. M., Maritan, L., & Cultrone, G. (2022). Firing and post-firing dynamics of mg- and ca-rich bricks used in the built heritage of the city of Padua (northeastern Italy). *European Journal of Mineralogy*, 34, 301–319. <https://doi.org/10.5194/ejm-34-301-2022>
- Picon, M., Carre, C., Cordoliani, M., Vichy, M., Hernandez, J., & Mignard, J. (1975). Composition of the La Graufesenque, Banassac and Montans Terra Sigillata. *Archaeometry*, 17, 191–199. <https://doi.org/10.1111/j.1475-4754.1975.tb00133.x>
- Piovesan, R., Dalconi, M. C., Maritan, L., & Mazzoli, C. (2013). X-ray powder diffraction clustering and quantitative phase analysis on historic mortars. *European Journal of Mineralogy*, 25, 165–175. <https://doi.org/10.1127/0935-1221/2013/0025-2263>
- Pradell, T., & Molera, J. (2020). Ceramic technology. How to characterise ceramic glazes. *Archaeological and Anthropological Sciences*, 12, 189. <https://doi.org/10.1007/s12520-020-01136-9>
- Pucci, G. (1973). La produzione della ceramica aretina. Note sull'“industria” nella prima età imperiale romana. In *Dialoghi di Archeologia* (Vol. 7) (pp. 255–293). Milano.
- Quinn, P. S. (2022). *Thin section petrography geochemistry & scanning electron microscopy of archaeological ceramics*. Archaeopress. <https://doi.org/10.2307/j.ctv2nwq8x4>
- Schindler-Kaudelka, E., Schneider, G., & Zabezhlicky-Scheffenecker, S. (1997). Les Sigillées padanes et tardo-padanes: nouvelles recherches en laboratoire. In Rivet L., *Proceedings of the Conference on Mans*, (Mans, 8–11 May 1997). Société Française d'Étude de la Céramique Antique en Gaule, Marseille, (pp. 481–494).
- Schneider, G., & Hoffmann, B. (1990). Chemische Zusammensetzung italischer Sigillata. In E. Ettliger (Ed.), *CRöm.-German. Komm. d. Dt. Archäolog. Inst. zu Frankfurt a. M., E. Ettliger u.a. (Materialien zur römisch-germanischen Keramik; H. 10)*, Bonn, (pp. 27–38).
- Schneider, G., & Zabezhlicky-Scheffenecker, S. (2016). *Sigillata from the insula II and a private house in the eastern quarter of Velia -chemical analysis and archaeological discussion*. In FACEM (version 16/16/12/2016) <http://www.facem.at>
- Sciau, P., Sanchez, C., & Gliozzo, E. (2020). Ceramic technology: How to characterize terra sigillata ware. *Archaeological and Anthropological Sciences*, 12, 211. <https://doi.org/10.1007/s12520-020-01137-8>
- Sternini, M. (2012). *La fortuna di un artigiano nell'Etruria romana*, Effigi edizioni, Arcidosso, p. 96.
- Toby, B. H. (2006). R factors in Rietveld analysis: How good is good enough? *Powder Diffraction*, 21, 67–70. <https://doi.org/10.1154/1.2179804>
- Trindade, M. J., Dias, M., Coroado, J., & Rocha, F. (2009). Mineralogical transformations of calcareous rich clays with firing: A comparative study between calcite and dolomite rich clays from Algarve, Portugal. *Applied Clay Science*, 42, 345–355. <https://doi.org/10.1016/j.clay.2008.02.008>
- Verde, M., De Bonis, A., Renson, V., Germinario, C., Rispoli, C., D'Uva, F., Tomeo, A., & Morra, V. (2022). Mineropetrographic characterization of fine ware from Cales (South Italy). *Archaeometry*, 65, 1–40. <https://doi.org/10.1111/arc.12873>
- Vitali, V., & Franklin, U. M. (1986). New approaches to characterization and classification of ceramics on the basis of their elemental composition. *Journal of Archaeological Science*, 13, 161–170. [https://doi.org/10.1016/0305-4403\(86\)90005-1](https://doi.org/10.1016/0305-4403(86)90005-1)
- Warr, L. (2021). IMA–CNMNC approved mineral symbols. *Mineralogical Magazine*, 85(3), 291–320. <https://doi.org/10.1180/mgm.2021.43>
- Widemann, F., Picon, M., Asaro, F., Michel, H., & Perlman, I. (1975). A Lyon branch of the pottery-making firm of Ateius of Arezzo. *Archaeometry*, 17, 45–59. <https://doi.org/10.1111/j.1475-4754.1975.tb00114.x>
- Zoppi, A., Lofrumento, C., Castellucci, E. M., Dejoie, C., & Sciau, P. (2006). Micro-Raman study of aluminium-bearing hematite from the slip of Gaul sigillata wares. *Journal of Raman Spectroscopy*, 37, 1131–1138. <https://doi.org/10.1002/jrs.1597>
- Zoppi, A., Lofrumento, C., Castellucci, E., & Sciau, P. (2008). Al-for-Fe substitution in hematite: The effect of low Al concentrations in the Raman spectrum of Fe₂O₃. *Journal of Raman Spectroscopy*, 39, 40–46. <https://doi.org/10.1002/jrs.1811>

How to cite this article: Mascaro, M. E., Cantisani, E., Ricci, M., Pallecchi, P., Vilucchi, S., Dalconi, M. C., & Maritan, L. (2024). The production of *terra sigillata* in Arezzo, Central Italy: an archaeometric investigation. *Archaeometry*, 1–21. <https://doi.org/10.1111/arc.13023>